Plasma Physics Reports, Vol. 28, No. 4, 2002, pp. 286–295. Translated from Fizika Plazmy, Vol. 28, No. 4, 2002, pp. 319–328.

PLASMA DYNAMICS

Numerical Modeling of the Dynamics of a Slow Z-Pinch

A. S. Kingsep*, V. E. Karpov, A. I. Lobanov**, Y. Maron***, A. A. Starobinets***, and V. I. Fisher*****

**Russian Research Centre Kurchatov Institute, pl. Kurchatova 1, Moscow, 123182 Russia*

***Moscow Institute of Physics and Technology, Institutskiĭ proezd 9, Dolgoprudnyĭ, Moscow oblast, 141700 Russia*

****Weizmann Institute of Sciences, Rehovot, Israel*

Received May 24, 2001; in final form, November 22, 2001

Abstract—A study is made of the method for numerical modeling of pulsed plasma systems by simultaneously solving two-temperature MHD equations and the equations of ionization kinetics. As an example, the method is applied to simulate a relatively slow moderate-density Z-pinch, whose dynamics is well studied experimentally. A specially devised two-dimensional computer code makes use of a promising technique of parallel modeling. *© 2002 MAIK "Nauka/Interperiodica".*

1. INTRODUCTION

In this paper, we present the results of numerical experiments aimed at modeling the dynamics of a moderate-density Z-pinch on characteristic time scales of about 600–700 ns [1–3]. The computer code devised for simulations is based on the hydrodynamic model developed in [4] and on the kinetic model describing the dynamics of ionization states [1]. In the experiments of [1–3], the pinch was created with the help of a ring nozzle with an electromagnetic valve in CO_2, which served as the standard working gas. Since our numerical experiments were based on one-fluid MHD theory, we considered a purely carbon gas jet. The main objective of our simulations was not only to reproduce the experimental results in detail but even more importantly to prove the feasibility of our combined method and to test numerical techniques. The reason is that the most informative methods for investigating pulsed plasmas (regardless of the way in which they are produced) are provided by spectroscopy and the most convenient objects in testing spectroscopic methods are Z-pinches, which ensure a sufficiently high radiation intensity and high reproducibility of results at relatively low cost of experiments.

2. MATHEMATICAL MODEL AND BRIEF DESCRIPTION OF THE NUMERICAL METHOD

The MHD part of the combined method assumes the solution of the following one-dimensional model equations of motion for a two-temperature one-fluid plasma in a magnetic field in dimensionless form:

$$\frac{d\rho}{dt} + \rho\frac{1}{r}\frac{\partial(rv_r)}{\partial r} = 0,$$

$$\frac{dv_r}{dt} = -\frac{1}{\rho}\left(\frac{\partial}{\partial r}\left(P + \frac{B^2}{8\pi}\right)\right) - \frac{B^2}{4\pi\rho r},$$

$$\frac{\rho}{A}\frac{d}{dt}(z_{\mathrm{eff}}\varepsilon_e + J(z_{\mathrm{eff}})) = -P_e\frac{1}{r}\frac{\partial(rv_r)}{\partial r} + \frac{1}{r}\left(\kappa_e r\frac{\partial T_e}{\partial r}\right) + \frac{\nu}{4\pi}\left(\frac{1}{r}\frac{\partial rB}{\partial r}\right)^2 - Q_r + Q_{ei}, \quad (1)$$

$$\frac{\rho}{A}\frac{d\varepsilon_i}{dt} = -P_i\frac{1}{r}\frac{\partial(rv_r)}{\partial r} + \frac{1}{r}\frac{\partial}{\partial R}\left(\kappa_i r\frac{\partial T_i}{\partial r}\right) - Q_{ei},$$

$$\frac{dB}{dt} = -B\frac{1}{r}\frac{\partial(rv_r)}{\partial r} - \frac{\partial}{\partial r}\left(\frac{1}{r}\frac{\partial rB}{\partial r}\right),$$

where Q_r is the radiative (bremsstrahlung) loss power and Q_{ei} is the power of collisional energy exchange between electrons and ions. The subscripts *e* and *i* refer to electrons and ions, respectively. Most of the notation is standard: P without the subscript is the total pressure (i.e., the sum of the partial pressures of plasma electrons and ions), and the function $J(z_{\mathrm{eff}})$ accounts for energy losses from ionization. The equations were nondimensionalized with respect to the following main scales: the time scale is $[t] = 10^{-7}$ s, the length scale is $[r] = 1$ cm, the mass density scale is $[\rho] = 10^{-3}$ g/cm^3, and the temperature (energy) scale is $[T] = 1$ keV. The plasma is described by the ideal gas equations of state:

$$P_e = 9.68\frac{\rho T_e z_{\mathrm{eff}}}{A}, \quad \varepsilon_e = 14.4T_e, \quad (2)$$

$$P_e = 9.68\frac{\rho T_i}{A}, \quad \varepsilon_i = 14.4T_i;$$

Here and below, A is the number of nucleons in a nucleus (the atomic weight). The model equations are written in dimensionless form. The power of collisional energy exchange between electrons and ions is

$$Q_{ei} = 8.48 \times 10^{-1} \frac{\rho^2 z_{\mathrm{eff}}^3}{A^3} \frac{T_i - T_e}{T_e^{3/2}}, \tag{3}$$

and the radiative loss power is

$$Q_r = 0.174 A^{-2} z_{\mathrm{eff}}^2 \rho^2 T_e^{0.5}. \tag{4}$$

The electron and ion thermal diffusivities are chosen to be

$$\begin{aligned} \kappa_e &= 2.21 \times 10^{-2} T_e^{2.5} z_{\mathrm{eff}}^{-1}, \\ \kappa_i &= 6.6 \times 10^{-4} T_i^{2.5} z_{\mathrm{eff}}^{-4} A^{-0.5}, \end{aligned} \tag{5}$$

and the magnetic viscosity has the form

$$\nu = 2.59 \times 10^{-5} z_{\mathrm{eff}} T_e^{-1.5}; \tag{6}$$

where z_{eff} is the effective ion charge number in the plasma. Our earlier studies showed that plasma magnetization at $\omega_{Be} \ll \omega_{pe}$ (or equivalently $B^2 \ll nmc^2$) has no significant effect on the macroscopic pinch dynamics. That is why we assumed that the plasma is unmagnetized, the more so because we were primarily interested in proving the feasibility of our combined method.

At the outer pinch boundary, we imposed the conditions corresponding to those at the boundary between a plasma and vacuum. In this case, the azimuthal magnetic field at the boundary is related to the total current in the external electric circuit by the familiar dimensionless relationship

$$B = \frac{0.2I(t)}{R},$$

where I is the current in the external circuit and R is the instantaneous radius of the corresponding point in the Z-pinch corona.

The above set of MHD equations was solved by the method of separation of the scales of the physical processes. In the first stage of calculations, the code takes into account the plasma motion and solves inviscid MHD equations without allowance for dissipative effects. The difference scheme is constructed using Lagrangian mass coordinates and provides the second-order approximation in the spatial variables. In order to reduce the oscillations that appear in calculating discontinuous solutions (such as shock waves and contact and tangential discontinuities), the pressure term is supplemented with an artificial viscosity term. The simulations were carried out with a combination of linear and quadratic viscosity coefficients [5]. The explicit, completely conservative difference schemes that were implemented computationally in the code are analogous to those described in [5]. The code also imposes restrictions on the minimum size of cells of the difference mesh. When the spatial dimension of one of the cells becomes smaller than the minimum allowable dimension, all of the quantities (specifically, not only the "traditional" parameters such as the plasma temperature, momentum, and mass but also the mean ion charge in the cell and radiative losses) are conservatively recalculated for a new mesh. Since an algorithm for such recalculation is fairly obvious, we do not describe it here. The numerical methods used in computations are quite similar to those applied in earlier papers [4, 6]. In the next stages of calculations, the code solves the equations for the electron and ion thermal diffusivities and the magnetic-field diffusion equation by the flux sweep methods [7]. In the final stage, the code takes into account the energy exchange between electrons and ions and also radiative losses. The sets of ordinary differential equations (ODEs) that are precisely determined in this stage of separation of the scales of the physical processes are solved by the method of trapezoids.

In each Lagrangian cell in each hydrodynamic time step (or several steps), the code integrates (on the intrinsic kinetic time scale) a set of 200–300 ODEs determining the population of the quantum states of plasma atoms and ions. All of the seven charge states of carbon atoms are taken into account. For the first six charge states, systematic account is taken of the lowest 20–40 terms for electron configurations with one or two excited electrons. The higher terms are modeled by Rydberg levels with the statistical weights taking into account all of the terms of the residual atomic core [8]. For each charge state, the Rydberg levels are used to model all higher-lying levels, up to the instantaneous effective boundary of the continuum; in turn, this boundary is usually calculated in the ion sphere approximation (and, more rarely, in the Debye–Hückel approximation) [9]. The effective decrease in statistical weights for higher-lying levels as the boundary energy of the continuum decreases [10] is neglected because of the contradictions between the approaches to estimating this effect quantitatively (see, e.g., [11, 12]). The model used in our simulations assumes that, as the energy of a discrete level becomes higher than the boundary energy of the continuum, all of the electrons occupying this level remain unbound. An increase in the ionization potential above its previous value (e.g., during plasma expansion) is accompanied by the reproduction (or appearance) of the higher lying discrete quantum states, whose population is calculated from the Saha–Boltzmann relationships, which are valid for all discrete levels adjacent to the boundary of the continuum [9, 13].

The set of kinetic equations describes the populations of all quantum states incorporated into the model and expresses each of the populations in terms of the instantaneous populations of the remaining quantum states and the probabilities for all possible quantum transitions. Under the thermodynamic conditions prevailing in small Z-pinches (in the case at hand, the plasma line density is up to 50 mkg/cm), the most probable transitions are spontaneous radiative transitions and transitions induced by free electrons. Transitions induced by the radiation field and ion impact are neglected because they are far less probable. The model incorporates the following one-electron processes: one-electron ionization (in the case at hand, the ejection of an electron from the outermost shell and from the nearest *nl* subshell, including ionization to the excited states [14, 15]) and transitions within the same charge state (collisional excitation and deexcitation as well as spontaneous radiative transitions).

For carbon, the data on the Grotrian diagrams for an atom and ions, the energies of the bonded states, the oscillatory forces, and the ionization potentials in vacuum are available in the NIST Atomic Database (http://physics.nist.gov/). In the computer code, the probabilities of all collision processes are expressed in terms of their cross sections for an arbitrary distribution function. In this paper, we present the results that were obtained only for a Maxwellian distribution function.

The cross sections for one-electron ionization are described by the semi-empirical formula [16], which is a refined version of the Lotz formula (see, e.g., [17]). Numerous comparisons with the results of quantum mechanical calculations showed that, to within 20%, the semi-empirical formula [16] yields the same ionization cross sections as the disturbed wave (DW) method, including the cross sections for ionizations from and to the excited states. The cross sections for the reverse processes (three-body recombination) are expressed through the ionization cross sections in accordance with the principle of detailed balance [18, 19], which is a consequence of the quantum mechanical reciprocity theorem [20]. The cross sections for multielectron ionization is calculated from the formula obtained in [21]. The cross sections for radiative recombination are described by the Milne formula [18, 19], which relates them to the associated photoionization cross sections, described, in turn, by the Kramers formula. It is well known that, for many-electron ions, the Kramers formula also provides a satisfactory degree of accuracy [9]. The dielectronic recombination is described in accordance with the monograph by Griem [9]. The cross sections for all of the excitation processes are calculated by L.A. Vainshtein's ATOM software program [22, 23], written on the basis of the Coulomb–Born method with allowance for exchange and renormalization. The excitation cross sections are included into the corresponding database and are then used to calculate the excitation probabilities. The cross sections for the reverse processes are expressed in terms of the excitation cross sections through the Klein–Rossealand formula [18, 19], which reflects the principle of detailed balance.

Previously, the model described here (or, more precisely, the corresponding model for a zero-dimensional Z-pinch) was tested by simulating different scenarios for plasma ionization. The software program devised for integrating the set of ODEs numerically is based on the Gear method [24] and includes the corresponding program module from the NAG library, which is widely used in computations. According to the present-day classification, the Gear method belongs to a class of the so-called "multivalued" methods. Given that the step of numerical integration is constant, the family of these methods is equivalent to the backward differentiation formulas [25–27]. The implicit backward differentiation formulas provide a high degree of approximation by the use of the results calculated at several preceding time steps, in which case, however, in several initial time steps, the set of ODEs should be integrated by some other numerical method. In contrast to these formulas, the Gear method starts to integrate the equations immediately from the first time step and has a variable order of approximation (convergence). At several initial time steps, it may have a somewhat lower order of convergence [25]. These intrinsic properties of the Gear method constitute its advantage in investigating the zero-dimensional model, because they make it possible to obtain solutions for different scenarios of the ionization of Z-pinch plasmas, including those at the limits of applicability of the physical model [21]. However, computer programs making allowance for ionization that were described in [21] are somewhat difficult to combine directly with the above MHD module of the code. In this context, the main advantage of the Gear method (namely, an algorithm for automatic choice of the time step, guaranteeing the desired accuracy) becomes unnecessary because the equations of ionization kinetics are integrated on a too short time scale and, accordingly, the mean degree of approximation decreases. On the other hand, the number of references to the subroutine integrating the set of kinetic equations is large.

In order to increase the mean order of convergence of the Gear method and to successfully carry out integration over the above initial time steps, the subroutine integrating the set of kinetic equations was called up after a fixed number of time steps. Note that, during the calculation of the processes occurring in a plasma, the time intervals after which the subroutine integrating the set of quantum mechanical equations was called up became progressively shorter. Simultaneously, the ionization processes being modeled became more rapid, thereby shortening the time integration step and, as a consequence, the time intervals after which the subroutine integrating the set of kinetic equations was called up.

The above features of the one-dimensional numerical method did not allow us to implement the two-dimensional method on sufficiently fine difference meshes, because a decrease in the spatial cell size leads to a proportional decrease in the time step and, consequently, worsens the approximation achievable in the calculation of ionization processes. Using implicit schemes does not improve the situation. The reason is that it is necessary to satisfy not only the Courant condition [28, 29] but also the following condition, which is important for a correct description of the physical processes incorporated into the model: in each time step, the perturbations in the pinch should propagate through no more than one Lagrangian cell. These restrictions could be overcome by using implicit schemes, but then the model of ionization processes would be incorrect. Nevertheless, the results obtained in our numerical experiments are of interest from the physical standpoint.

3. NUMERICAL RESULTS FROM THE ONE-DIMENSIONAL MODEL

We simulated a Z-pinch in a carbon plasma. The line pinch density was in the range from 0.006 to 0.01 mg/cm, and the initial pinch radius was 2.6 cm. These values are close to the experimental data of [1–3]. We did not solved the electric-circuit equation but instead interpolated the experimental dependence of the total current in the circuit [1–3]. This dependence is well approximated by a straight line corresponding to a current rise time of 610 ns and a peak current of 300 kA. Because of the large amount of calculations, we succeeded in tracing all stages of the Z-pinch evolution on a mesh consisting of only 30 cells. A typical scenario for the pinch evolution can be described as follows. Initially (during a time interval of about 200 ns), the plasma is essentially at rest. The plasma of the liner is slightly heated only in the nascent corona (a low-density current-carrying plasma region), and this process is accompanied by a small increase in the effective ion charge number. In the remaining liner regions, the initial ion charge number (0.9) is somewhat different from its equilibrium value at these densities and temperatures, so that the effective ion charge number also increases only slightly (up to 0.93) and the plasma electron temperature decreases from 2 to 1.6–1.8 eV. At about 200 ns after the switching-on of the current, the liner starts moving, in which case the plasma is largely concentrated near the outer pinch boundary and the corona practically disappears; i.e., the "snowplow" effect is observed.

Figure 1 illustrates the time evolution of the radial profiles of the plasma mass density in the pinch. The profiles shown in Fig. 1a were obtained at 0, 150, 225, and 300 ns in the initial stage, during which the liner

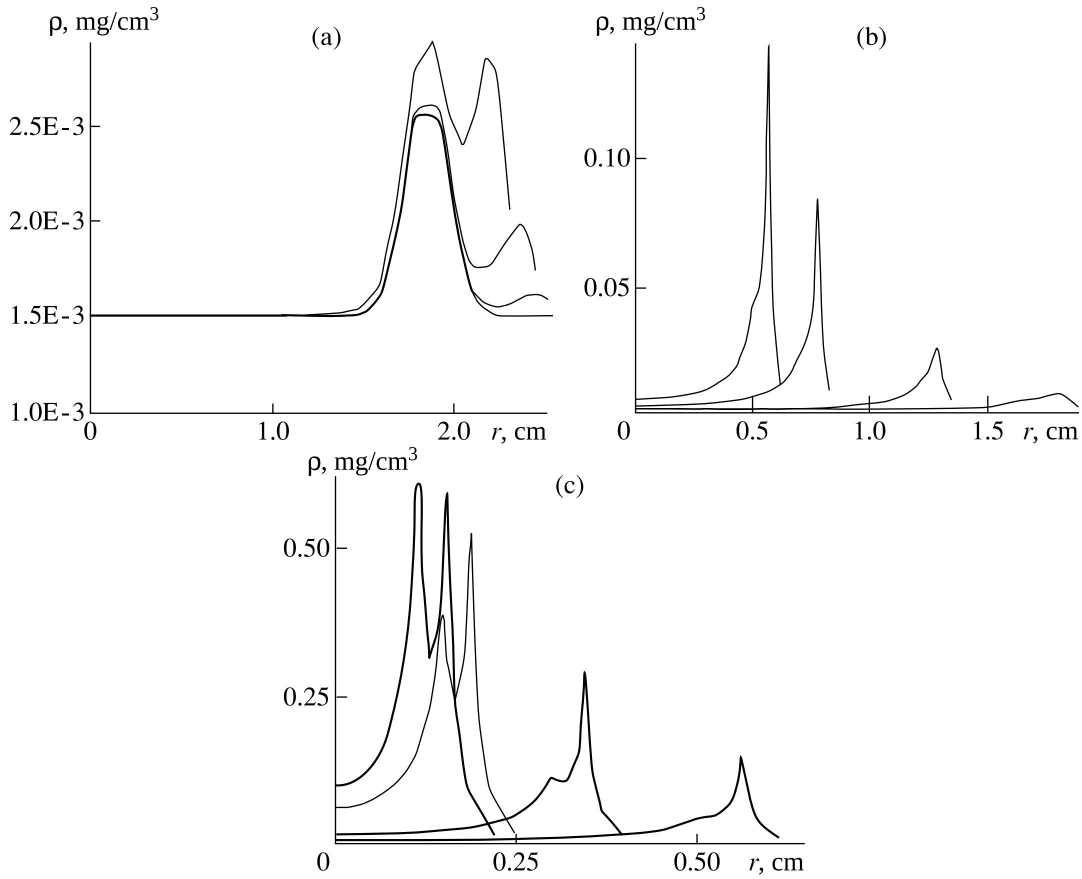

Fig. 1. Radial profiles of the plasma mass density obtained in the plasma compression stage and in the initial stage of plasma expansion. The profiles in Fig. 1a were calculated at 0, 150, 225, and 300 ns. The profiles in Fig. 1b were calculated at 420, 510, 570, and 590 ns. The profiles in Fig. 1c were calculated near the time of maximum compression, i.e., at 610, 630, and 655 ns (from right to left). The profile calculated at the time when the plasma starts expanding (690 ns) is shown by a light curve.

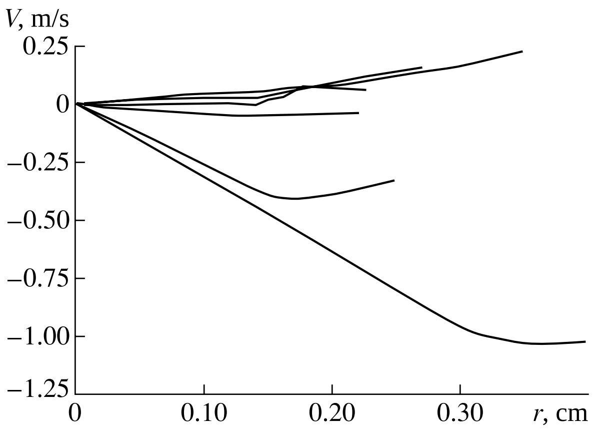

Fig. 2. Radial profiles of the plasma velocity calculated at 610, 630, 655, 690, 730, and 770 ns (from top to bottom).

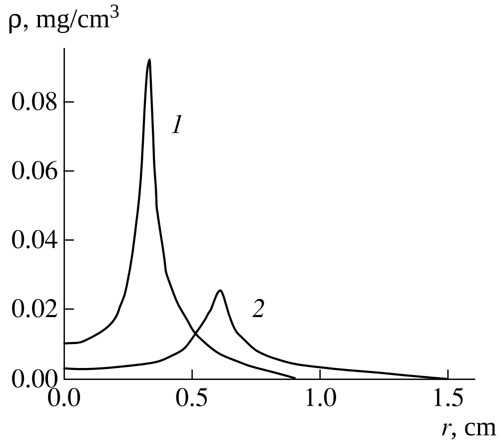

Fig. 3. Radial profiles of the plasma mass density obtained in the stage of plasma expansion (at 970 and 1170 ns).

plasma is at rest. At later times (up to about 550 ns), the plasma is compressed in essentially the same manner. The plasma mass is mostly accumulated in the snowplow region. The profiles shown in Fig. 1b were obtained at 420, 510, 570, and 590 ns. We can see that, after 550 ns, a shock wave forms ahead of the snowplow region.

Figure 1c shows the radial profiles of the plasma mass density calculated at 610, 630, 655, and 690 ns, i.e., over the time interval from the instant at which the current in the external electric circuit is switched on (610 ns) to the instant at which the plasma starts to expand (690 ns). The profile corresponding to the latter instant is shown by a light curve. We can clearly see the reflection of a shock wave from the pinch axis and the formation of an entropic layer [7], in which the plasma temperature is elevated and the plasma density is depressed. Such entropic effects are an undesirable feature of the numerical methods used to solve the MHD equations. The entropic layer is present throughout all subsequent stages of calculations and, as will be shown below, decreases the reliability of the results obtained in the stage of plasma expansion.

At the time of maximum compression, all the liner plasma is essentially comes to a stop. Figure 2 shows the radial profiles of the plasma velocity calculated at 610, 630, 655, 690, 730, and 770 ns. We can see that, at 650 ns, the plasma is practically at rest, and, at 690 ns, it expands with a certain positive velocity. A discontinuity in the plasma velocity is associated with the reflection of the shock wave from the outer boundary of the liner. The representative radial profiles of the plasma mass density in the expansion stage (at 970 and 1170 ns) are shown in Fig. 3. The plasma velocity is uniform along the pinch radius, the maximum velocity at 1170 ns is about 3 cm/ms, and the radius of the entropic layer, which is present as before, is now about 5–6 mm.

Figure 4 illustrates the time evolution of the radial profiles of the electron and ion temperatures. The profiles were calculated at 610, 630, 655, and 690 ns. It is notable that the ion temperature in the entropic layer increases considerably (from 1300 to 4000 eV). The possible causes of this phenomenon will be discussed below. The ion temperature values behind the shock wave seem to be quite realistic (from 300 to 800 eV). This is also true for the electron temperature values in the main plasma (from 50 to 80 eV) and in the corona (from 100 to 350 eV).

Note that, at these times, the plasma is ionized almost completely, except in the maximum density region, in which the mean ion charge number is about five. The dynamics of the mean ion charge number in the plasma at earlier times (at 420, 510, 570, and 590 ns) is illustrated in Fig. 5. The ion charge in the corona increases because, at such electron temperatures, the magnetic field does not penetrate into the plasma, but rather is completely concentrated in the skin layer. Under these conditions, the Joule heating of the plasma in the skin layer plays an important role: in particular, it increases the mean ion charge. Initially, an increase in the mean ion charge ahead of the skin layer is associated with the effects of electron heat conduction, and later, with the combined action of electron heat conduction and the heating by a propagating shock wave.

Unfortunately, a completely developed shock wave affects the course of calculations: it slightly decreases the reliability of the results computed in the stage of plasma expansion.

We now address the question of the temperature increase immediately before the focusing of the shock wave at the pinch axis. This increase can only be explained as being due to the formation of one more (weaker) shock wave, which was focused at the axis at an earlier time and was not captured numerically because the time intervals after which the calculated results were read into computer memory were too large.

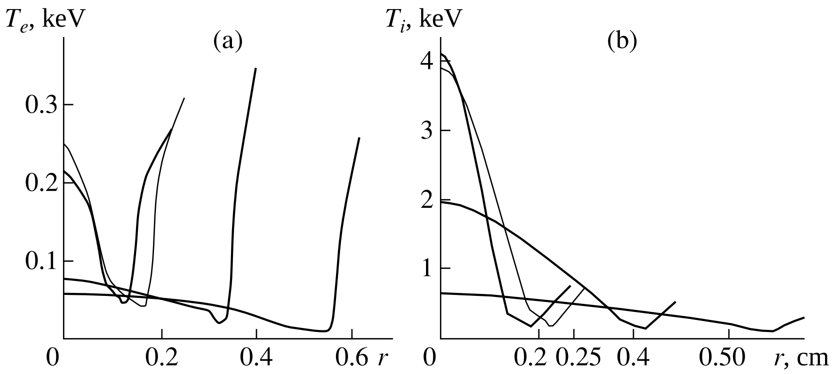

Fig. 4. Dynamics of the (a) electron and (b) ion temperatures. The radial profiles were calculated at 610, 630, and 655 ns. The profiles calculated at the time when the plasma starts expanding (690 ns) are shown by the light curves.

Such a wave does indeed exist and was captured in the simulations of a pinch with a line density of 0.01 mg/cm and with small values of the artificial viscosity coefficients on the difference mesh.

Because of the larger mass of the pinch, it was compressed on a somewhat longer time scale (about 695 ns). Figure 6 shows the radial profiles of the effective ion charge number, plasma mass density, and electron and ion temperatures calculated at 670 and 690 ns.

In the case of a liner with a line density of 0.01 mg/cm, the time 690 ns coincides not only with the time at which a weaker shock wave starts to form but also with the time at which the previous shock wave is reflected from the axis. On the calculated profiles, one can see the nascent entropic layer and oscillations stemming from the small artificial viscosity used in the simulation of the liner under consideration. The oscillations are most pronounced in the radial profile of the electron temperature. The oscillations of the effective ion charge number result from those of the electron temperature.

Another interesting effect revealed in simulations is that the electron temperature and effective ion charge number oscillate in a fixed Lagrangian cell. Such small-amplitude periodic variations in the electron temperature in a fixed cell were observed between 300 and 500 ns in essentially all of the calculation versions. Unexpectedly, this effect was also captured by two-dimensional modeling.

4. RESULTS OF TWO-DIMENSIONAL SIMULATIONS

Here, we describe the results of modeling of a pinch with a line density of 0.006 mg/cm, an initial radius of 2.6 cm, and a length of 2.6 cm. The pinch was initiated in a carbon gas between two electrodes, which were assumed to be "cold" (in simulations, their temperature was set equal to zero) and impenetrable by the plasma. The corresponding boundary conditions for Eqs. (1)–(5) were chosen to be analogous to those used in [4].

Up to 500 ns, a two-dimensional pinch evolves in the same manner as a one-dimensional pinch, the only difference being that the plasma temperature near the cold electrodes is slightly depressed. The discrepancy between the evolutions becomes significant on longer time scales. The depressed temperature of the electrode plasmas (Fig. 7) gives rise to a slight longitudinal (in the z-direction) plasma inhomogeneity, which is enhanced by oscillations of the plasma temperature and of the effective ion charge number. As a result, two inward-directed plasma jets form at a distance of about 0.3 cm from each of the electrodes. The jets are distinctly seen in the ion pressure distribution in Fig. 8 and in the projections of the isolines of the plasma mass density in Fig. 9.

Figures 7–9 show the distributions calculated at 630 ns, at which time two jets reach the symmetry axis (Fig.

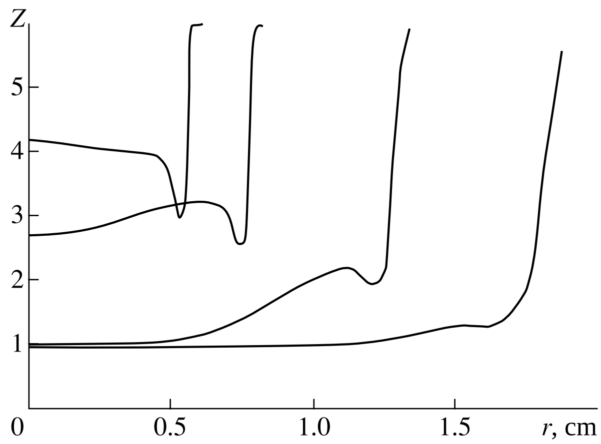

Fig. 5. Radial profiles of the mean ion charge calculated in the liner compression stage (at 420, 510, 570, and 590 ns).

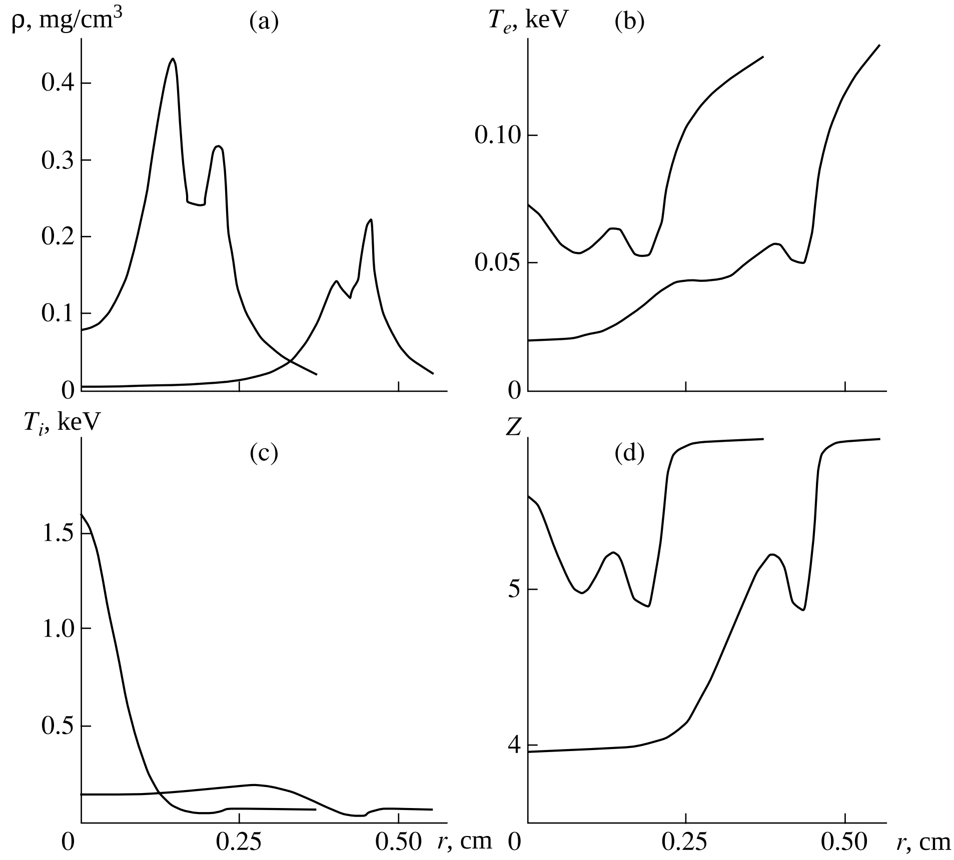

Fig. 6. Reflection of a shock wave from the axis and formation of a subsequent shock wave during the evolution of a pinch with a line density of 0.01 mg/cm. The radial profiles of the (a) plasma mass density, (b) electron and (c) ion temperatures, and (d) mean ion charge number were calculated at 670 and 690 ns. At 670 ns, the position of the shock front (at about 1 mm) is most clearly seen in the electron temperature profile. The entropic layer is seen to develop at 690 ns.

8) and the third jet forms in the main pinch just between the electrodes. This jet is seen in both the ion pressure (Fig. 8) and plasma mass density (Fig. 9) distributions. It appears in the region of elevated electron temperature.

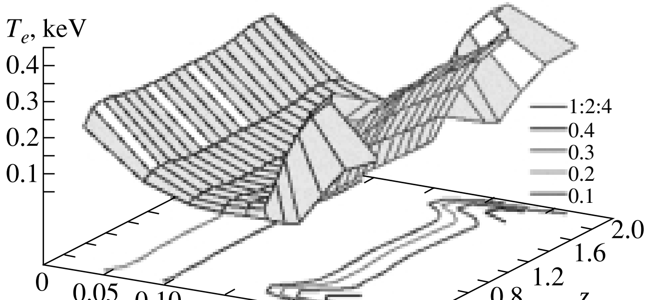

Fig. 7. Electron temperature distribution in two-dimensional modeling.

After the jet reaches the pinch axis, the electron and ion temperatures in the axial region increase. The calculated results show that the ion temperature increases to a significant extent, specifically up to 6–7 keV, which is high in comparison with the ion temperature in the "cold" regions (4 keV). However, such a significant increase is only associated with the entropic effects. In the electron temperature distribution, similar hot points appear somewhat later. They are associated with the energy exchange between very hot ions and comparatively cold electrons and are less pronounced than those in the ion temperature distribution. The presence of hot points at the pinch axis can be established primarily from the calculated ion pressure distribution, because the ion pressure is least sensitive to the entropic effects.

Unfortunately, we failed to obtain the two-dimensional picture of plasma motion on time scales longer than 670 ns.

On time scales of up to 500 ns, the perturbations of the outer pinch boundary were found to result only in slight deviations from the evolution of a one-dimensional pinch.

5. USE OF THE CLUSTER OF PERSONAL COMPUTERS FOR TWO-DIMENSIONAL SIMULATIONS

Estimates show that, with present-day single-processor personal computers (PCs), numerical integration of two-dimensional problems on fine meshes (containing from 60×134 to 100×204 Lagrangian cells) usually takes from a week to a month of computer time. Because of this, it is desirable to exploit parallel computers. Since most of computer time (up to 90%) is expended on simulating the kinetic (quantum mechanical) part of the problem, it is expedient to parallel only kinetic calculations, whereas the hydrodynamic processes and magnetic field diffusion can be simulated, as before, on a single-processor PC.

Even with the semiautomatic estimation of the run time of the program (™BERT77, the trademark of Paralogic, Inc., http://www.plogic.com), it was not possible to estimate the total time required to execute it, because the cycles in the program are organized so that it terminates only when the prescribed accuracy is achieved. In order to estimate the actual efficiency of using a parallel computer, we carried out some test measurements in solving the kinetic part of the problem on the above difference mesh under the Linux operating system on a PC with a Celeron-366 microprocessor. On the average, this part took 27 minutes of computer time. That the kinetic part can be calculated for each Lagrangian cell independently opens great possibilities for using parallel computers. In order to distribute the kinetic calculations almost equally between 12 processors in a PC cluster, the difference mesh was divided into 12 equal components in the radial direction. The choice of the direction was dictated by the fact that the main perturbations (shock waves) propagate from the periphery of the plasma toward its center, so that, with such a division of the plasma region, the processors handle approximately equal number of Lagrangian cells adjacent to the shock front.

The execution of the remaining part of the program requires that the amount of information exchanged between the PCs be 280 KB, which takes less than one second.

Estimates showed that, on a PC cluster organized in this way, calculating the kinetic part of the problem takes about 2.5 minutes. With allowance for the time required to execute all of the moduli of the program, the cluster completes the problem 10.8 times faster than does a single-processor PC.

Let us consider some of the results from two-dimensional simulations on a PC cluster. The results again refer to a pinch with a line density of 0.006 mg/cm, an initial radius of 2.6 cm, and a length of 2.6 cm, but now the simulations were carried out on a finer mesh. The pinch was initiated in a carbon gas between two electrodes, which were assumed to be "cold" (in simulations, their temperature was set equal to zero) and impenetrable by the plasma. In order to describe the

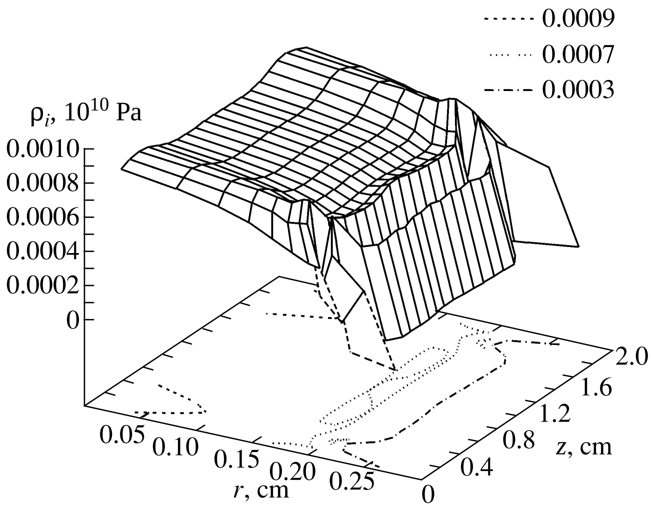

Fig. 8. Ion pressure distribution and the initial stage of the formation of hot points at the axis in two-dimensional modeling.

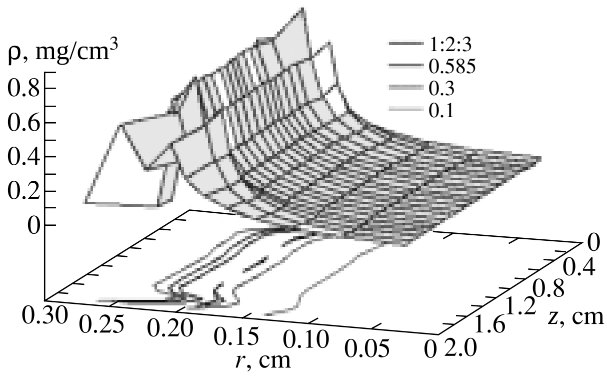

Fig. 9. Distribution of the mass density of a plasma compressed to one-tenth of its initial volume.

effects of the Rayleigh–Taylor instability, the conditions imposed at the right boundary of the plasma region specified a small sinusoidal perturbation with an amplitude of 0.25 to 5% of the initial pinch radius. The problem was solved on meshes containing from 60×134 to 100×206 Lagrangian cells, and the corresponding calculations on a 12-PC cluster took from 24 to 48 hours.

In order to illustrate the effects revealed in simulations, we present the electron and ion temperature distributions calculated for a pinch whose right boundary was perturbed sinusoidally at an amplitude of about 2.5% of the initial pinch radius. The temperature distributions obtained from two-dimensional simulations on a fine mesh are shown graphically in Fig. 10, in which only each fourth point obtained in every direction is plotted. We can see that the compression proceeds in

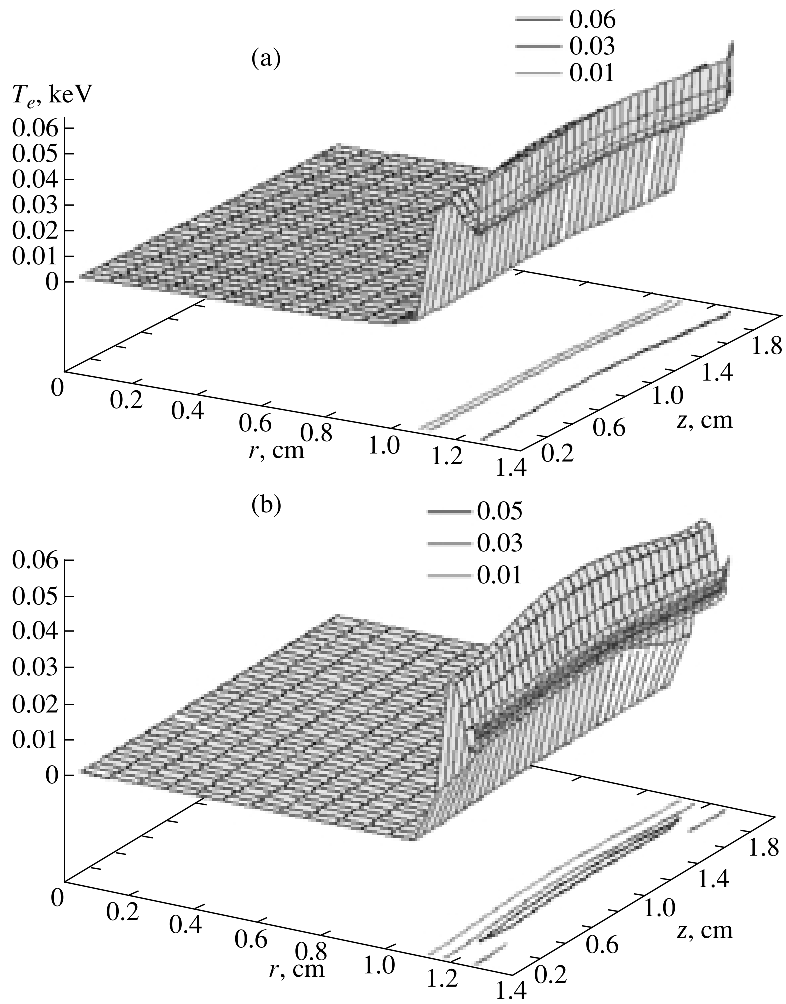

Fig. 10. Electron and ion temperature distributions calculated on a fine (60 × 134) mesh on a PC cluster at 450 ns (only some of the calculated points are plotted). Small-scale structures are seen to appear near the cooled electrode.

essentially the same way as in the above one-dimensional case. On such time scales, the Rayleigh–Taylor instability does not affect the compression of the liner. Nonetheless, small-scale structures are seen to appear near the electrodes (Fig. 10). The PC cluster was capable of handling the problem on time scales of about 500–510 ns. On longer time scales, the simulations were terminated because of the rapid deformation of the Lagrangian mesh near the cooled electrode.

6. CONCLUSIONS

An analysis of the results of our one- and two-dimensional simulations show that we can speak of the formation of a high-density plasma layer and its subsequent transformation into a shock wave. Although our numerical experiments provide indirect evidence for such behavior of an imploding plasma, they cannot give a detailed information about the underlying mechanisms that cause it. It is also of interest to point out the role of the supersonic propagation of the ionization front: presumably, it is this factor that is responsible for the destruction of a shock wave.

Note that our main results were obtained on fairly rough meshes, containing from 17 × 17 to 27 × 47 Lagrangian cells. On a mesh with 30 cells, one-dimensional calculations of all the stages of the process (compression, pinching, and plasma expansion) on time scales of about 1200 ns require 60–80 hours of computer time on a PC with a Celeron-366 microprocessor; moreover, about 90% of this time is expended on simulating the kinetic (quantum mechanical) part of the problem. Even with very rough meshes, two-dimensional simulations of the pinch evolution up to the stage of maximum compression require at least 100 hours. The progress toward the development of the models combining hydrodynamic and quantum mechanical approaches is expected to be made through increased use of parallel computers. That this way is promising is evidenced, in particular, by the results of our work.

ACKNOWLEDGMENTS

This work was supported in part by the Israeli Academy of Sciences and Arts, INTAS (grant no. 97-0021), and the Russian Foundation for Basic Research (project no. 01-01-00401).

REFERENCES

1. M. E. Foord, Y. Maron, G. Davara, *et al.*, Phys. Rev. Lett. **72**, 3827 (1994).
2. M. E. Foord, Y. Maron, G. Davara, *et al.*, Phys. Rev. Lett. **73**, 1190 (1994).
3. G. Davara, L. Gregorian, E. Kroupp, and Y. Maron, Phys. Plasmas **5**, 1068 (1998).
4. Yu. G. Kalinin, A. S. Kingsep, V. I. Kosarev, and A. I. Lobanov, Mat. Model. **12** (11), 47 (2000).
5. A. A. Samarskiĭ and Yu. P. Popov, *Difference Methods for Solving Gas Dynamics Problems* (Nauka, Moscow, 1992, 3rd ed.).
6. A. S. Kingsep, V. I. Kosarev, A. I. Lobanov, and A. A. Sevast'yanov, Fiz. Plazmy **23**, 953 (1997) [Plasma Phys. Rep. **23**, 879 (1997)].
7. R. P. Fedorenko, *Introduction to the Computer Physics* (MFTI, Moscow, 1994).
8. L. M. Biberman, V. S. Vorob'ev, and I. T. Yakubov, *Kinetics of Nonequilibrium Low-Temperature Plasmas* (Nauka, Moscow, 1982; Consultants Bureau, New York, 1987).
9. H. R. Griem, *Principles of Plasma Spectroscopy* (Cambridge Univ. Press, Cambridge, 1997).
10. V. E. Fortov and I. T. Iakubov, *Physics of Nonideal Plasma* (Inst. Khim. Fiz., Chernogolovka, 1984; Hemisphere, New York, 1990).
11. R. M. More, Adv. At. Mol. Phys. **21**, 305 (1985).
12. D. G. Hummer and D. Michalas, Astrophys. J. **331**, 794 (1988).
13. H. R. Griem, *Plasma Spectroscopy* (McGraw-Hill, New York, 1964; Atomizdat, Moscow, 1969).
14. D. H. Sampson, Phys. Rev. A **34**, 986 (1986).
15. M. E. Foord and E. Nardi, J. Appl. Phys. **68**, 5028 (1990).
16. V. A. Bernshtam, Yu. V. Ralchenko, and Y. Maron, J. Phys. B **33**, 5025 (2000).
17. S. M. Younger and T. D. Mark, in *Electron Impact Ionization*, Ed. by T. D. Mark and G. H. Dunn (Springer-Verlag, New York, 1985).
18. I. I. Sobelman, L. A. Vainshtein, and E. A. Yukov, *Excitation of Atoms and Broadening of Spectral Lines* (Springer-Verlag, Berlin, 1995).
19. J. Oxenius, *Kinetic Theory of Particles and Photons* (Springer-Verlag, Berlin, 1986).
20. L. D. Landau and E. M. Lifshitz, *Quantum Mechanics: Non-Relativistic Theory* (Nauka, Moscow, 1989; Pergamon, New York, 1977).
21. V. I. Fisher, Yu. V. Ralchenko, A. A. Goldgrish, *et al.*, J. Phys. B **28**, 3027 (1995).
22. V. P. Shevelko and L. A. Vainshtein, *Atomic Physics for Hot Plasmas* (Inst. of Physics Press, Bristol, 1993).
23. V. I. Fisher, Yu. V. Ralchenko, V. A. Bernshtam, *et al.*, Phys. Rev. A **55**, 329 (1997).
24. D. Kahaner, C. Moler, and S. Nash, *Numerical Methods and Software* (Prentice-Hall, Englewood Cliffs, 1989; Mir, Moscow, 1998).
25. E. Hairer, S. Norsett, and G. Wanner, *Solving Ordinary Differential Equations*, Vol. 1: *Nonstiff Problems* (Springer-Verlag, Berlin, 1987; Mir, Moscow, 1990).
26. E. Hairer and G. Wanner, *Solving Ordinary Differential Equations*, Vol. 2: *Stiff and Differential-Algebraic Problems* (Springer-Verlag, Berlin, 1996; Mir, Moscow, 1999).
27. A. Nordsieck, Math. Comput. **16**, 22 (1962).
28. S. K. Godunov and V. S. Ryaben'kiĭ, *Difference Schemes* (Nauka, Moscow, 1977).
29. D. A. Anderson, J. C. Tannehill, and R. H. Pletcher, *Computational Fluid Mechanics and Heat Transfer* (Hemisphere, New York, 1984; Mir, Moscow, 1990), Vols. 1, 2.

Translated by O. E. Khadin

SPELL: inviscid